International Journal of Nanoelectronics and Materials
IJNeaM
ISSN 1985-5761 | E-ISSN 2232-1535

Synthesis and Characterization of Lithium-doped $BaTiO_3$/Si(100) Thin Films with Variations of 0 %, 0.5 %, 1 % and 1.5 % as Potential Forerunners of Solar Cells

Nurhidayah[a*], Samsidar 1[a], Frastica Deswardani 2[a], Mardian Peslinof 3[a], R M Anggraini 4[a], M F Afrianto 5[a], Irzaman 5[b], Muhammad Dahrul 6[b], Meilini Rahmani 7[b], Anis Munir Rukyati 8[b] and Ridwan Siskandar 9[c*]

[a] *Physics Department, Jambi University, Jambi, Indonesia;*
[b] *Physics Department, IPB University, Bogor, West Java 16680, Indonesia;*
[c] *Computer Engineering Technology Study Program, College of Vocational Studies, IPB University, Bogor, West Java 16151, Indonesia;*
∗Corresponding author. e-mail: nurhidayah@unja.ac.id; ridwansiskandar@apps.ipb.ac.id

Received 27 November 2022, Revised 30 August 2023, Accepted 15 September 2023

ABSTRACT

Thin films of $BaTiO_3$/Si(100) in Lithium with doping variations of 0%, 0.5%, 1%, and 1.5% were successfully grown on a p-type Si substrate using Chemical Solution Deposition method. The films were annealed at 850 °C for 15 hours. The crystal structure was characterized using X-Ray Diffraction (XRD) with Material Analysis Using Diffraction (MAUD), Scanning Electron Microscope- Energy Dispersive X-Ray (SEM-EDX), optical absorption, and current – voltage (I-V) as potential solar cells. The results showed that the addition of Lithium doping affected the value of the lattice parameters and formed tetragonal crystals. The characterization results show that the bandgap energy value of the thin film due to lithium doping reduces the bandgap energy value because the donor atom added to a semiconductor causes the allowable energy level to be slightly below the conduction band. The presence of this new band causes the thin film bandgap energy to decrease with a five-valent tantalum dip. The morphological properties showed that the $BaTiO_3$/Si(100) thin film particles in the deposited Lithium had a reasonably homogeneous grain. With the addition of lithium acetate as a binder into barium titanate, the grain size is getting smaller because it is suspected that the lithium-ion radius is smaller than the barium-ion radius. Measurement of I-V on the thin film shows that the output voltage value increases with more light intensity hitting the surface of the thin film. The greater the light intensity, the greater the energy of the photons, so the electrons are easier to jump. The three things above (both electrical and morphological properties) conclude that the thin films grown have the potential for solar cells.

Keywords: *$BaTiO_3$/Si(100), Crystal Structure, Li(CH_3COO), Solar Cells, Thin Films*

1. INTRODUCTION

Ferroelectric materials are one of the interesting advanced materials research topics because of their wide application in various fields. One of the popular ferroelectric materials is Barium Titanate ($BaTiO_3$; BTO). Barium titanate was chosen as the material for the ferroelectric film because it has a high dielectric constant and a low Curie temperature (±120 ^{0}C) [1]–[3]. BTO ferroelectric material is a group of perovskite minerals with an ABX3 structure, where A and B are metallic elements, while X is a non-metallic element. The ferroelectric properties of the perovskite material stem from the shift of B ions along the c-axis from the centrosymmetric position of the unit cell, which causes a permanent electric dipole [4]. The total charge of ions A and B must be +6, with different atomic sizes, where the smaller ion, with the more significant charge, is a transition metal. In $BaTiO_3$, the Ba^{2+} ion occupies position A and Ti^{4+} in position B. The bond between the Ba^{2+} cation and the TiO_3 group is ionic, while a covalent bond between Ti and O atoms is formed [5].

Barium Strontium Titanate (BST) is a well-studied perovskite ferroelectric material in the form of thin films. Ferroelectric properties can be generated by making the BST thin films sensitive to light (optoelectronics), temperature stimuli (pyroelectric), and pressure effects (piezoelectric) [1], [6], [7]. The BST has been applied as an optoelectronic photodiode [8]. Also, light sensitivity has been used for automatic drying models in agriculture [1]. Furthermore, to change the properties of BST thin films, such as the lattice constant, dielectric constant, pyroelectric properties, optoelectrical properties, and piezoelectric properties, must be added by dopant. There are two types of dopants according to their elements. First, the soft dopant ions can make ferroelectric materials have a high elasticity coefficient, low coercive field properties, and lower mechanical quality factor. Second, the hard dopant ions can produce harder ferroelectric materials such as lower dielectric loss, lower bulk resistivity, higher coercive field properties, higher mechanical quality factor, and higher electrical quality factor [9], [10].

Several techniques have investigated synthetic BT thin films like sputtering, laser ablation, and sol-gel process [11]–[15]. On the other hand, BT thin films have been made by several techniques like dip-coating, vacuum evaporation, a sputtering process, and chemical solution deposition (CSD). The CSD method has good stoichiometric

control, easy to fabricate, and can be synthesized at room temperature [9], [16]–[18].

The container for $BaTiO_3$ material is essential in the electronic equipment fabrication process because it can change the ferroelectric characteristics as needed. Several parameters that are affected by the addition of doping include the energy gap value, dielectric constant, wavelength absorbance spectrum, and crystal characteristics. In Anindy's research [19], adding a filler has been shown to affect the thin film's lattice parameters, refractive index, and piezoelectric constant.

In general, fabricating a thin layer of Barium Titanate or perovskite can be done by physical and chemical methods [7], [20]. The stages of the research method carried out include (i) making thin films of BTO with 0%, 0.5%, and 1% Lithium (I) Acetate ($Fe(CH_3COO)$) (BLTO) with CSD method assisted by spin coating and making contact aluminium on BLT thin films [6], [21], (ii) tested X-Ray Diffraction (XRD) with Material Analysis Using Diffraction (MAUD), Scanning Electron Microscope (SEM) and (Energy Dispersive X-Ray (EDX) devices.

2. MATERIAL AND METHODS

2.1. Tools and Materials

Thin films of $BaTiO_3$/Si(100) in Lithium have been made by using p-type silicon (Si) substrate (100), Barium titanate ($BaTiO_3$) powder, Barium oxide (BaO) powder, Lithium acetate powder [$Li(CH_3COO)$, 99%], solvent 2-methoxy ethanol [C3H8O2, 99%], Aquabides, Methanol, Acetone, and dish soap. Furthermore, the equipment used in this research was insulated boxes, double-sided tape, solution, paper labels, stationery, scissors, solution bottles, diamond blades, tweezers, weighing paper, digital balance, gloves, masks, micropipettes, tissue, aluminium foil, stirrer, spatula, Branson Ultrasonic cleaner, XRD, Nabertherm Furnace, Ultraviolet Visible (UV-Vis) Spectrophotometer, SEM-EDX.

2.2. Thin Film Synthesis Procedure

2.2.1 Substrate Preparation

A diamond blade cut the substrate to 1.2 cm x 1.2 cm. Then, the substrate was weighed by digital balance (AS type R1 PLUS) with repetitions for each substrate. After that, the substrate was cleaned with aquabides solution with dish soap, methanol, and acetone. Substrate cleaning consists of 3 stages with different solutions using an ultrasonic cleaner. The cleaning time for each step was about 5-10 minutes. Also, the substrate must be dried with a hotplate before cleaning it with another solution.

2.2.2 Solution Preparation

The solution was prepared by using powdered $BaTiO_3$, BaO, powdered Lithium acetate [$Li(CH_3COO)$, 99%], and solvent 2-methoxy ethanol [$C3H8O_2$, 99%]. The ingredients were weighed according to the composition of the elements. The material that had been considered was put into a solution bottle. After that, the stirring process was carried out using a magnetic stirrer for 60 minutes. The solution was prepared with a variation of 0%, 0.5%, 1%, and 1.5% in 4 bottles of different solutions according to the composition in Table 1.

Table 1 Composition of materials for making $BaTiO_3$ solution at a solubility of 1 M

Variation Container	$BaTiO_3$/Si (100) (g)	BaO (g)	$Li(CH_3COO)$ (g)	2-methoxy ethanol (ml)
0%	0.4664	0	0	2
0.5%	0.4594	0.0046	0.0020	2
1%	0.4594	0.0046	0.0040	2
1.5%	0.4594	0.0046	0.0060	2

2.2.3 Thin Film Growth

The thin film was prepared using the CSD method with the spin coating technique. The silicon substrate was placed on a spin coater plate using double-sided tape. Half of the substrate was covered by tape, and the part not covered with tape was dripped with the previously prepared solution. The spin coater was rotated with a rotating speed setting at 3000 rpm for 60 seconds.

2.2.4 Annealing Stage

The annealing process aims to diffuse the thin film solution and a silicon substrate. The heating process began at room temperature and then raised to 850 ºC with an increased rate of 1.67 ºC/minute, then held constant at that temperature for 8 hours. Then the temperature was returned to room temperature. Raising the room temperature to 850 ºC takes approximately 8.5 hours, and it takes 12 hours to lower it back to room temperature.

2.3. Thin Film Synthesis Procedure

2.3.1 X-Ray Diffraction (XRD) with MAUD

The X-ray diffraction method was used to analyze a material's crystal structure, lattice constant, phase change, and crystallinity [11], [22]. The principle of XRD was based on X-ray diffraction, which is the scattering of light of a wavelength when passing through a crystal lattice with a distance between the angle of incidence and the crystal plane d [23]. In this study, the angle of XRD measurement for 2θ has an interval from 20 ° to 80 °, with an interval of 0.02 °/minute. The lattice parameter has been analyzed by using the Cramer and Cohan equations. MAUD Software was used to analyze the XRD data to determine the crystal size of each material phase.

2.3.2 SEM-EDX Test

The surface area of thin films has been investigated by SEM test with the magnification of 7500 times. The EDX test was carried out to determine what elements were contained in the thin film that had been synthesized in this study.

3. RESULTS AND DISCUSSION

3.1 Tools and Materials

XRD data analysis with the MAUD device aims to match the obtained diffraction pattern data with reference data. XRD data analysis using the Rietveld method with five iterations resulted in a graph of the smoothed $BaTiO_3$/Si(100) film diffraction pattern. Figures 1, 2, 3, and 4 are the results of XRD spectral data analysis, and the lattice parameter values are also obtained, as shown in Table 2. Figures 1, 2, 3, and 4 are XRD data experimentally smoothed with the MAUD method at the 6 peaks. Especially for the 0.5% Li(CH_3COO) light, the intensity at the 6 peaks of the crystal structure decreases (not disappears). It is suspected that the incorporation of 0.5% Li(CH_3COO) into the $BaTiO_3$/Si(100) film causes the prepared orientation of the 6 peaks of the crystal structure to shrink due to ionic-ionic site occupations (Ba^{2+}, Ti^{4+}, O^{2-} and Li^{1+}).) on $BaTiO_3$/Si(100) films with 0.5% Li(CH_3COO) changed, which caused the 6 peaks of the XRD experiment and the XRD with the MAUD smoothing method to decrease.

While adding 1% and 1.5% Li(CH_3COO) to $BaTiO_3$/Si(100) films, the intensity at the 6 peaks of the crystal structure increased again. It is suspected that the ions (Ba^{2+}, Ti^{4+}, O^{2-} and Li^{1+}) at 1% and 1.5% Li(CH_3COO) are more than ionic (Ba^{2+}, Ti^{4+}, O^{2-} and Li^{1+}) at 0.5% Li(CH_3COO)) per cell perovskite unit. It causes the prepared orientation of the 6 peaks of the crystal structure to enlarge due to the site occupation of the ions (Ba^{2+}, Ti^{4+}, O^{2-} and Li^{1+}) on $BaTiO_3$/Si(100) films with 1% and 1.5% Li(CH_3COO)) increased which caused the 6 peaks of the XRD experiment and XRD with the smoothing of the MAUD method also to increase.

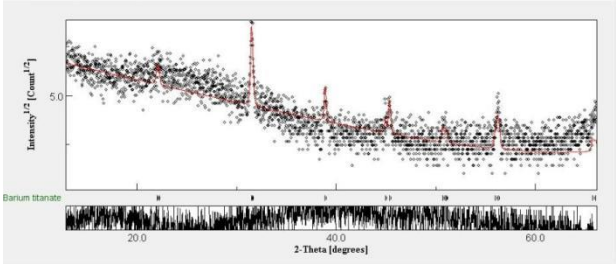

Figure 1. Diffraction pattern of $BaTiO_3$/Si(100) film without receptacle

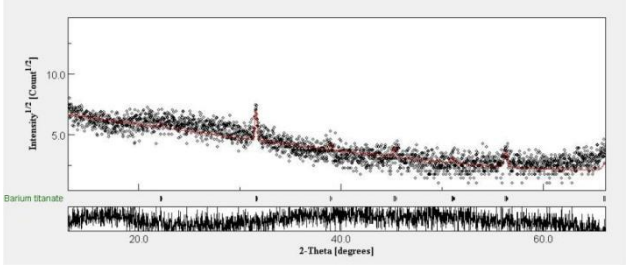

Figure 2. $BaTiO_3$/Si(100) film diffraction pattern with 0.5% Li(CH_3COO)

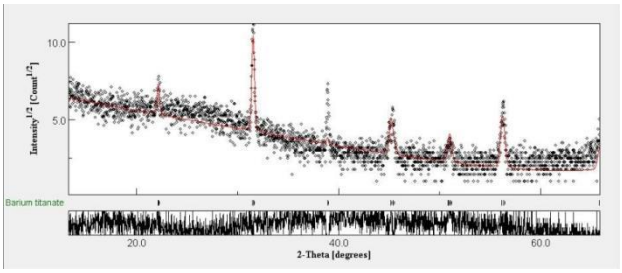

Figure 3. Diffraction pattern of $BaTiO_3$/Si(100) films with 1% reagent Li(CH_3COO))

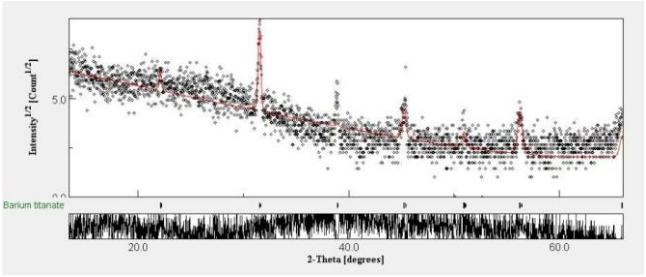

Figure 4. Diffraction pattern of $BaTiO_3$/Si(100) films with 1.5% reagent Li(CH_3COO))

Table 2 shows the lattice parameter values from the International Centre for Diffraction Data (ICDD) and MAUD literature. The lattice parameter values obtained from the MAUD device are almost close to the lattice parameter values in the ICDD literature.

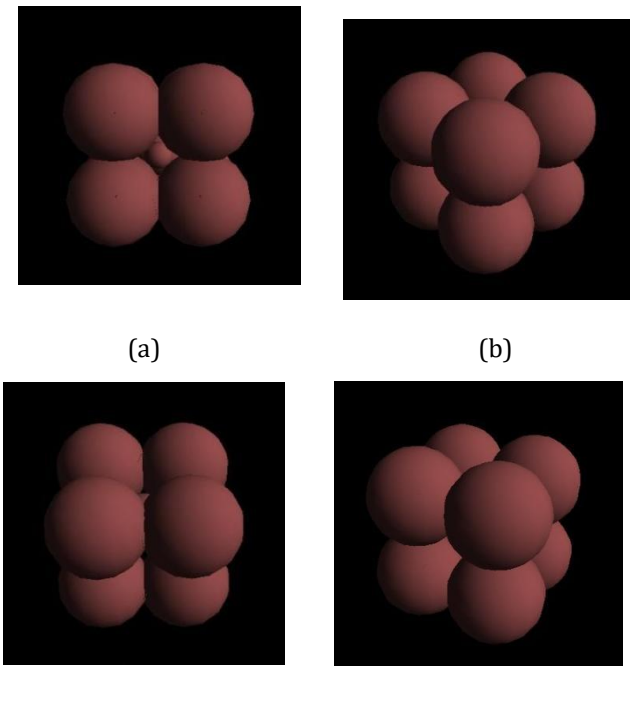

(a) (b)

(c) (d)

Figure 5. The structural form of BaTiO3/Si(100) with a reservoir (a) 0% Li(CH_3COO); (b) 0.5% Li(CH_3COO); (c) 1% Li(CH_3COO); and (d) 1.5% Li(CH_3COO)

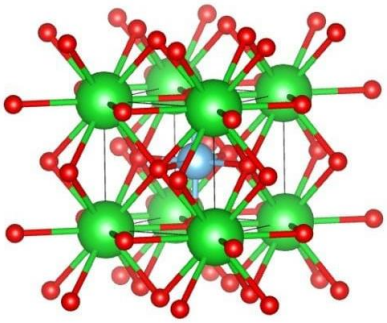

Figure. 6. The structural form of $BaTiO_3$/Si(100) using Vesta software (The green ionic Ba^{2+} is located in the corner of the perovskite unit cell. The blue ionic Ti^{4+} is located in the space centre unit cell perovskite. The red ionic O^{2-} is located in field diagonals perovskite unit cell)

Figure 5 shows the shape of the $BaTiO_3$/Si(100) film structure using the MAUD device, where the crystal structure of the $BaTiO_3$/Si(100) film is tetragonal. While Figure 5 shows the $BaTiO_3$/Si(100) structure using VESTA. Figure 6 also describes the atomic positions in the system. The green atom indicates the barium atom, the blue atom shows the titanium atom, and the red atom indicates the oxygen atom.

Table 2 Lattice parameters of $BaTiO_3$/Si(100) thin film with tetragonal structure $Li(CH_3COO)$ using MAUD

Variation	ICDD literature (Å)		MAUD Grid Parameters	
	a	c	a	c
0%	3.994	4.038	3.996	4.032
0.5%			4.006	4.032
1%			4.012	4.009

3.2. Energy Gap

The energy gap was obtained by plotting curve $(ahv)^2$ against the photon energy. Figure 7 shows the value of the intersection of the touch plot line with the x-axis, which is the energy gap value. The energy gap value has decreased with the addition of $Li(CH_3COO)$, leading to an increase in the thin film's electrical conductivity. When a donor atom is added to a semiconductor, the permissible energy level will be slightly below the conduction band. The presence of this new band causes the thin film bandgap energy to decrease with five-valent lithium doped [21]. Previous research has stated that the energy gap can increase after adding a lithium filler [24] [25].

As a result of dissolving 0.5%, 1%, and 1.5% $Li(CH_3COO)$ into $BaTiO_3$/Si(100) films it causes a decrease in the value of the energy gap (although very small/less significant) per perovskite cell unit. It is suspected that in perovskite unit cells, the most active group is TiO6 with an octahedron structure where there is an electron configuration between Ti^{4+} ions in the 3d subshell and O^{2-} ions in the 2s subshell. So with the addition of 0.5%, 1%, and 1.5% $Li(CH_3COO)$ into $BaTiO_3$/Si(100) films, the decreasing energy gap can be seen.

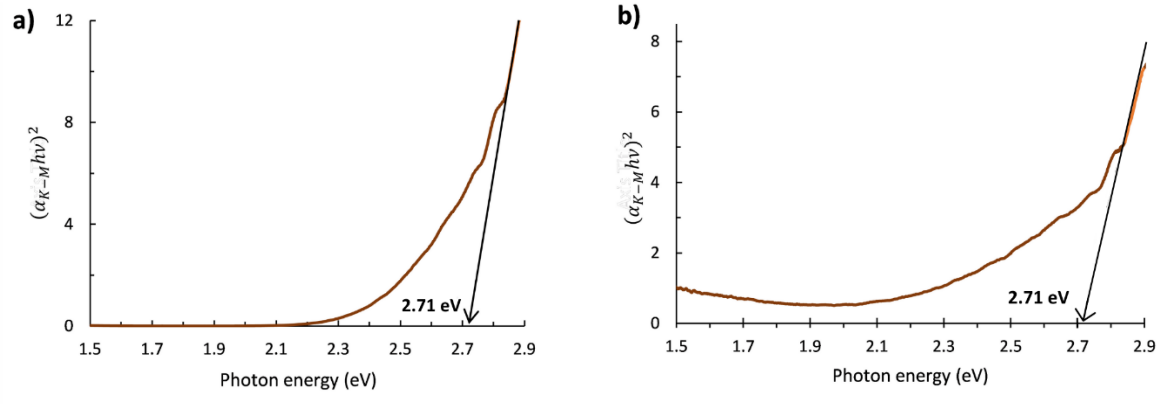

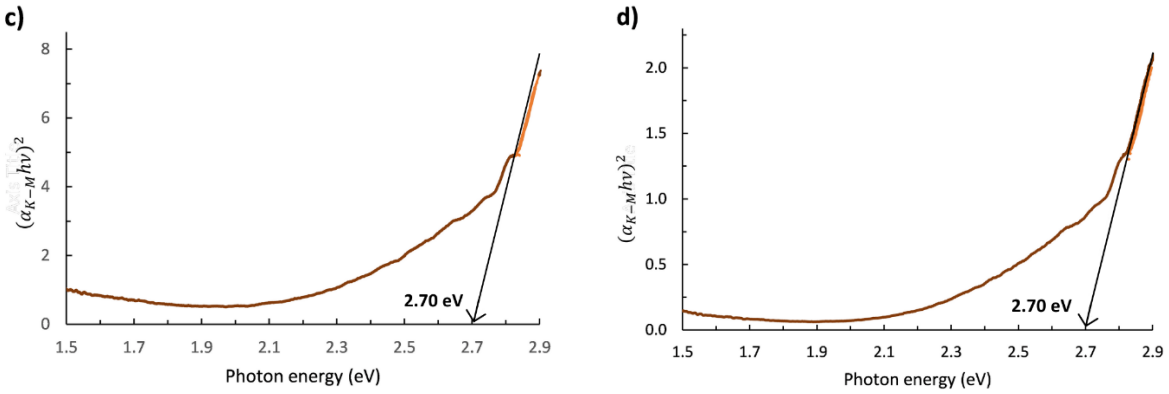

Fig. 7. Energy Gap: (a) 0% $Li(CH_3COO)$; (b) 0.5% $Li(CH_3COO)$; (c) 1% $Li(CH_3COO)$; and (d) 1.5% $Li(CH_3COO)$

3.3. SEM/EDAX Analysis

The result of SEM has shown the morphological structure of $BaTiO_3/Si(100)/Si(100)$ thin films in Lithium. The surface morphology of a material and grain size (grain) can be analyzed. The surface morphology of the $BaTiO_3/Si(100)/Si(100)$ thin film in Lithium is shown in Figures 8, 9, 10, and 11. These figures show that the $BaTiO_3/Si(100)$ thin film particles in the deposited Lithium have fairly homogeneous grains.

Figure 8 shows that the particle diameter of the $BaTiO_3/Si(100)$ thin film in Lithium is about 0.2 nm. Figure 9 shows that the particle diameter size of the $BaTiO_3/Si(100)$ thin film in Lithium is about 0.19 nm. Figure 10 shows that the particle diameter of the $BaTiO_3/Si(100)$ thin film in Lithium is about 0.17 nm. Figure 11 shows that the particle diameter size of the $BaTiO_3/Si(100)$ thin film in Lithium is about 0.16 nm. The addition of lithium acetate as a binder into barium titanate resulted in a smaller grain size because it was suspected that the lithium-ion radius was smaller than the barium-ion radius.

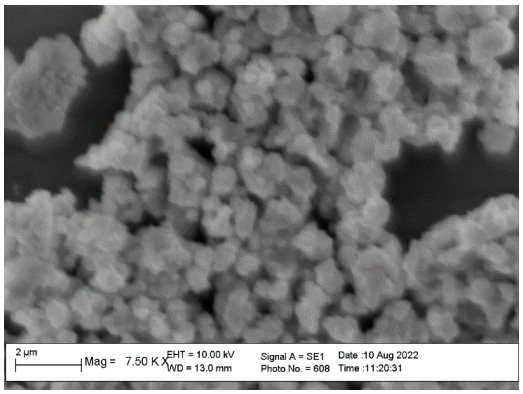

Figure 8. Morphology of the $BaTiO_3/Si(100)$ thin film particles not exposed to Lithium with a magnification of 7500 times the SEM image

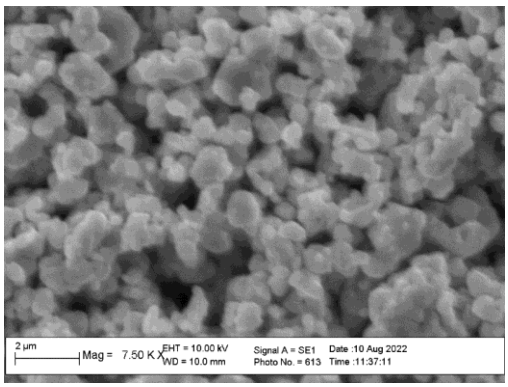

Figure 9. Morphology of $BaTiO_3/Si(100)$ thin film particles treated with 0.5% Lithium with a magnification of 7500 times the SEM image

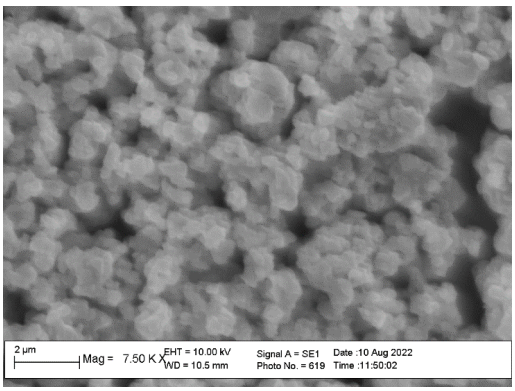

Figure 10. Morphology of $BaTiO_3/Si(100)$ thin film particles in 1% Lithium dispersed with a magnification of 7500 times the SEM image

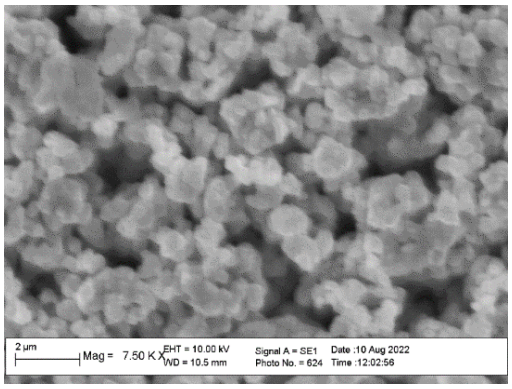

Figure 11. Morphology of $BaTiO_3$/Si(100) thin film particles in 1.5% Lithium dispersed with a magnification of 7500 times the SEM image

Figures 12, 13, 14 and 15 show the EDX results of a thin film of $BaTiO_3$/Si(100) in Lithium tincture.

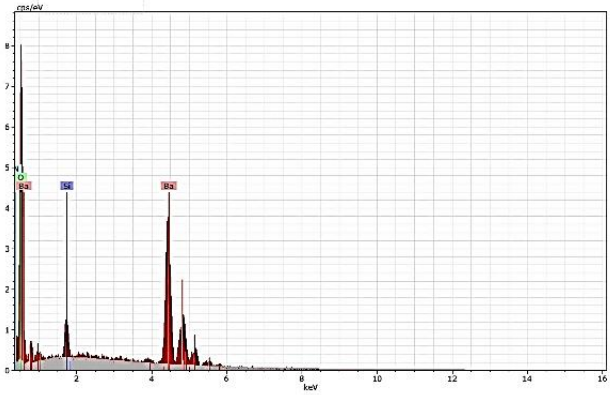

Spectrum: Acquisition 118

Element	Series	unn. C [wt.%]	norm. C [wt.%]	Atom. C [at.%]	Error [%]
Barium	L-series	45.76	43.03	8.04	2.7
Oxygen	K-series	49.14	46.20	74.09	12.0
Silicon	K-series	2.14	2.01	1.83	0.2
Nitrogen	K-series	9.31	8.76	16.04	3.5
Total:		106.35	100.00	100.00	

Figure 12. Composition of materials contained in a thin film layer of $BaTiO_3$/Si(100) without Lithium

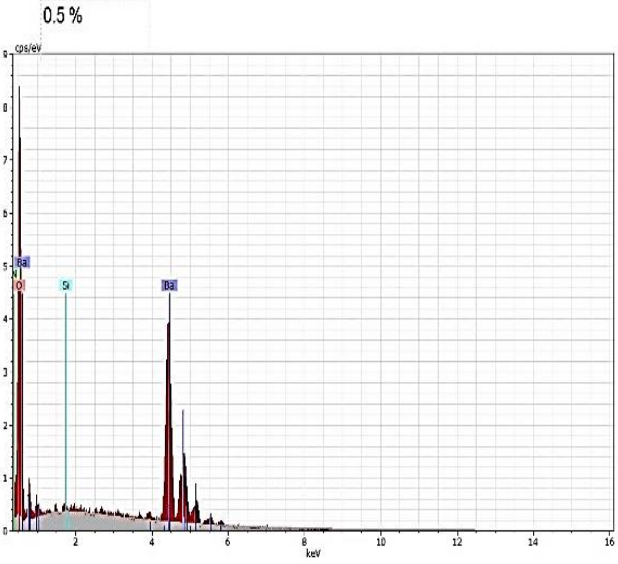

Spectrum: Acquisition 119

Element	Series	unn. C [wt.%]	norm. C [wt.%]	Atom. C [at.%]	Error [%]
Oxygen	K-series	49.72	48.82	75.82	12.1
Nitrogen	K-series	9.44	9.26	16.43	3.5
Barium	L-series	42.45	41.68	7.54	2.5
Silicon	K-series	0.24	0.23	0.21	0.1
Total:		101.85	100.00	100.00	

Figure 13. The composition of the material contained in a thin film layer of $BaTiO_3$/Si(100) prepped with 0.5% Lithium

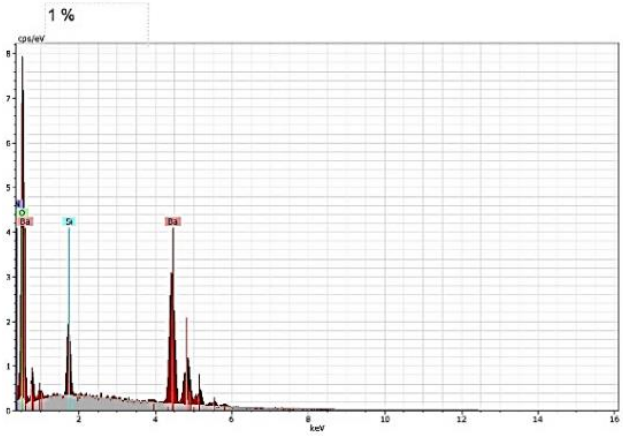

Spectrum: Acquisition 120

Element	Series	unn. C [wt.%]	norm. C [wt.%]	Atom. C [at.%]	Error [%]
Barium	L-series	35.36	37.04	6.45	2.1
Oxygen	K-series	51.19	53.63	80.20	12.4
Nitrogen	K-series	6.02	6.31	10.78	2.6
Silicon	K-series	2.00	3.02	2.57	0.3
Total:		95.46	100.00	100.00	

Figure 14. Composition of materials contained in a thin film layer of $BaTiO_3$/Si(100) on 1% Lithium

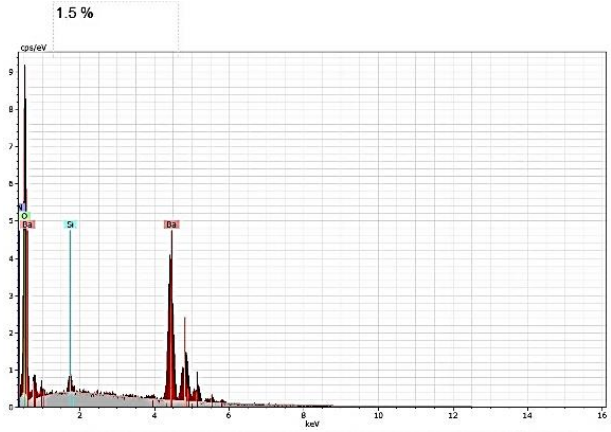

Spectrum: Acquisition 121

Element	Series	unn. C [wt.%]	norm. C [wt.%]	Atom. C [at.%]	Error [%]
Barium	L-series	37.70	39.71	7.07	2.2
Oxygen	K-series	50.43	53.12	81.22	12.2
Nitrogen	K-series	5.92	6.23	10.09	2.5
Silicon	K-series	0.89	0.94	0.82	0.1
Total:		94.93	100.00	100.00	

Figure 15. Composition of materials contained in a thin film layer of $BaTiO_3$/Si(100) on 1.5% Lithium

The EDX results in Figures 12, 13, 14, and 15 do not get lithium atoms because the lithium atoms have a small atomic number, so the EDX does not capture the energy emitted by Lithium. The EDX results in Figure 12 show that the composition of the material contained in the $BaTiO_3$/Si(100) thin film in Lithium is 43.03% Ba, 2.01% Si, 8.76% N, and 46.20% O. The EDX results in Figure 13 show that the composition of the material contained in the $BaTiO_3$/Si(100) thin film in Lithium is 41.68% Ba, 0.23% Si, 9.26% N, and 48.82% O. The EDX results in Figure 14 show that the composition of the material contained in the $BaTiO_3$/Si(100) thin film in Lithium is 37.04% Ba, 3.02% Si, 6.31% N, and 53.63% O. Figure 15 shows that the composition of the material contained in the $BaTiO_3$/Si(100) thin film in Lithium is 39.71% Ba, 0.94% Si, 6.23% N, and 53.12% O. More specifically, the atomic composition of the EDX results is shown in Table 3.

The results of this EDX analysis show that the $BaTiO_3$/Si(100) film is not stoichiometric because the lithium atom has a small atomic number, so the EDX does not capture the energy emitted by Lithium.

Table 3. The atomic composition of the EDX results

Lithium container (%)	Li (%)	Ba (%)	O (%)	Si (%)	N (%)
0	can not be read	43.03	46.20	2.01	8.76
0.5	can not be read	41.68	48.82	0.23	9.26
1.0	can not be read	37.04	53.63	3.02	6.31
1.5	can not be read	39.71	53.12	0.94	6.23

3.4. The thin film of $BaTiO_3$/Si(100) in lithium diode has the potential as a solar cell

Based on the result of the electrical and morphological properties of $BaTiO_3$/Si(100) thin films with 0%, 0.5%, 1%, and 1.5% lithium, it shows that thin films with 1.5% lithium doping were the best films and high potential for implementation as solar cells. The solar cells made of $BaTiO_3$/Si(100) thin film in Lithium 1.5% were done by adding aluminum contacts on a substrate of silicon Si(100) and barium titanate so that the structure of Al/$BaTiO_3$/Si(100) was formed. The arrangement of solar cells resembles a sandwich, as shown in Figure 16. Furthermore, the current and voltage characterization of the solar cell samples has been carried out using an ammeter and voltmeter.

The current-voltage (I-V) characterization has been done in two conditions: with light and without light. When a solar cell is exposed to sunlight, there will be a generation of what? (the emergence of electron-hole pairs). The photons absorbed by the electrons on the surface cause the electrons to be excited, and then the electrons flow toward the?? through the metal contact layer.

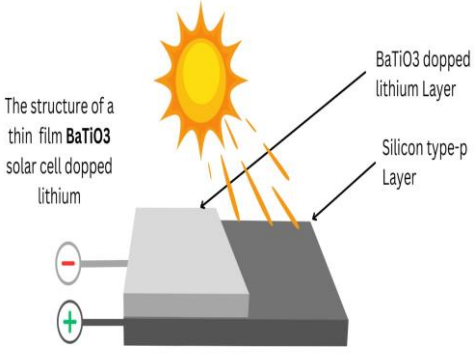

(a)

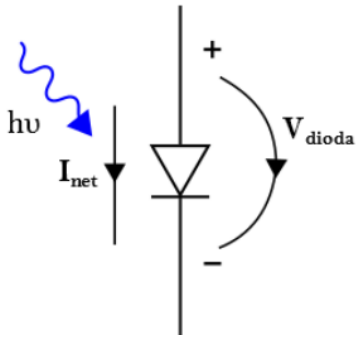

(b)

Figure 16. The arrangement of solar cells: (a) $BaTiO_3$/Si(100) thin film-based solar cell structure in Lithium; (b) Electronic circuit of I-V curve characterization (without and with illumination)

The metal contact layer became a pathway for electrons to flow faster toward holes. Then, the electrons flow through the external load to the counter electrode and the?? accepted by the electrolyte. When the holes form, they will diffuse into the electrolyte. Electrons will recombine with the hole to form negative charge carriers.

Table 4 shows the voltage measurement results; the stress value increased when Lithium was added to the film layer. The I-V measurements were carried out without light (0 lux) and with light (130000 lux ≃ 1000 Wm^{-2}), where 1 lux is 7.90 mW/m2 [26] [27] [28]. Table 4 shows that Votlage Open Circuit (Voc), Short Circuit Current Density (Jsc), Fill Factor (FF) and efficiency increase with additional doping. Table 4 shows that 1.5% doping produces the highest efficiency value compared to other doping, which is 0.65% (see curve I-V Figure 18(j) to determine the value of Voc= 2.60 volts, Isc= 0.40 mA, Vm (maximum voltage) = 2 volts, Im (maximum current) = 0.33 mA, while the formula for obtaining the efficiency value is shown in Equation 1. The FF value is 0.63, so that it can be obtained by 0.65% at a light intensity of 130000 lux ≃ 1000 Wm^{-2} with a solar cell with an area of 1 cm^2). The intensity of the light is proportional to the energy of the photons, so the electrons

jump more easily. This shows that films with 1.5% doping have the potential to be better as solar cells than other films.

$$FF = \frac{V_{MPP}.I_{MPP}}{V_{OC}.I_{SC}}$$
$$P_{MAX} = V_{OC}.I_{SC}.FF \quad (1)$$
$$\eta = \frac{P_{MAX}}{P_{radiance} \times A} \times 100\%$$

with FF is Fill Factor, Vmpp is maximum power point Voltage, Impp is maximum power point Current, Voc is open circuit Voltage, Isc is short circuit, Pmax is maximum power, η is efficiency, Pradiance is radiance power and A is surface area.

Besides Table 4, the results of the solar cell simulator measurements (doping 1.5%, 10000 lux) are also presented, as shown in Figure 17. The results of the simulator and the results of measurements using a multimeter produce the same value.

Based on the results of XRD pattern analysis using MAUD, the gap energy from the optical properties test, SEM/EDAX analyzers, and I-V measurement results of thin-film solar cells from the electrical properties test, it shows that the $BaTiO_3$/Si(100) thin films in Lithium have potential as solar cells.

In this case, the I-V curve when the $BaTiO_3$/Si(100) thin films in Lithium were given light stimulation and no light stimulation (dark), was also studied. The researcher did this in 4 samples (0% (Fig. 18(a);(b) and (c)), 0.5% (Fig. 18(d);(e) and (f))), 1% (Fig. 18(g)) ;(h) and (i)) and 1.5%(Figure 18(j);(k) and (l))) where each was repeated three times. PMore specifically, the I-V curve of the solar cell is shown in Figure 18.

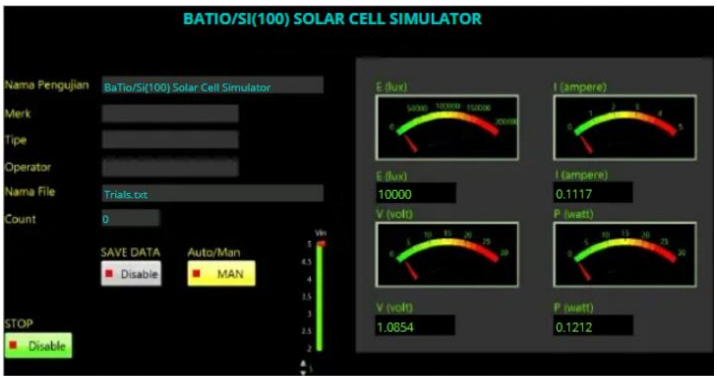

Figure 17. Solar cell simulator dashboard

Table 4 I-V measurement results of thin-film solar cells

Cell	Repetition	V_{oc} (V)	J_{sc} (mAcm^{-2})	FF	η (%)
0% Li(CH_3COO)	1	1.60	1.54 x 10^{-5}	0.36	0.88 x 10^{-5}
	2	1.80	0.90 x 10^{-5}	0.70	1.14 x 10^{-5}
	3	1.00	0.50 x 10^{-2}	0.72	0.36 x 10^{-5}
0.5% Li(CH_3COO)	1	1.40	0.50 x 10^{-2}	0.56	3.92 x 10^{-3}
	2	1.50	2.40 x 10^{-3}	0.11	0.40 x 10^{-3}
	3	1.60	0.20 x 10^{-5}	0.50	1.60 x 10^{-3}
1% Li(CH_3COO)	1	2.60	0.90 x 10^{-5}	0.60	1.40 x 10^{-5}
	2	2.50	0.90 x 10^{-5}	0.72	1.63 x 10^{-5}
	3	2.60	1.54 x 10^{-5}	0.34	1.35 x 10^{-5}
1.5% Li(CH_3COO)	1	2.60	0.40	0.63	0.65
	2	2.60	0.24	0.63	0.39
	3	2.60	0.24	0.63	0.39

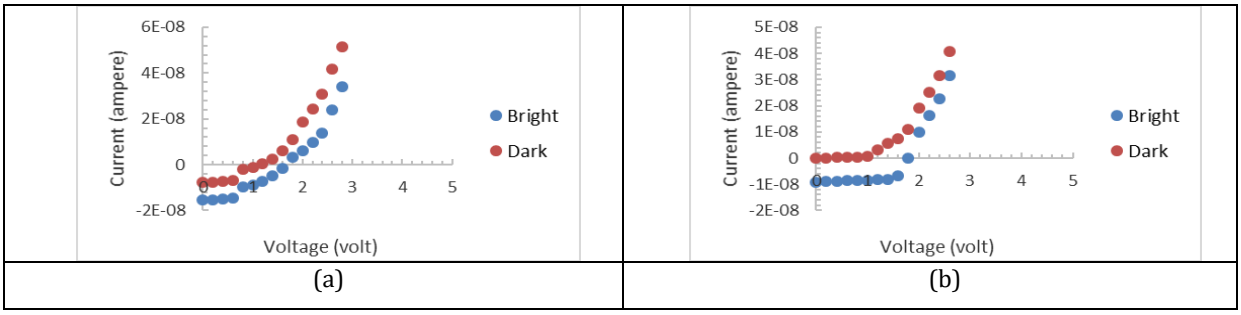

(a) (b)

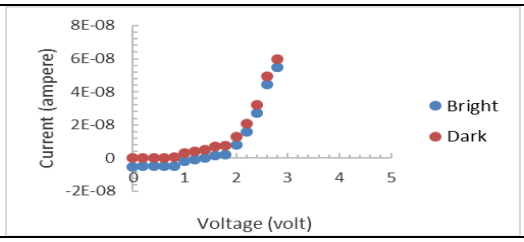
8E-08
6E-08
4E-08
2E-08
0
-2E-08
Current (ampere)
0 1 2 3 4 5
Voltage (volt)
Bright
Dark

(c)

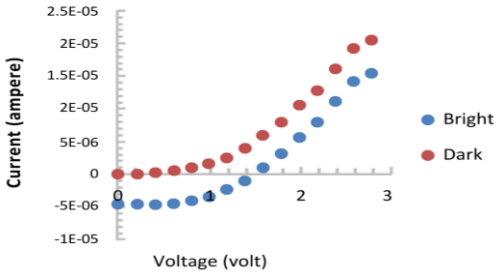
2.5E-05
2E-05
1.5E-05
2E-05
5E-06
0
-5E-06
-1E-05
Current (ampere)
0 1 2 3
Voltage (volt)
Bright
Dark

(d)

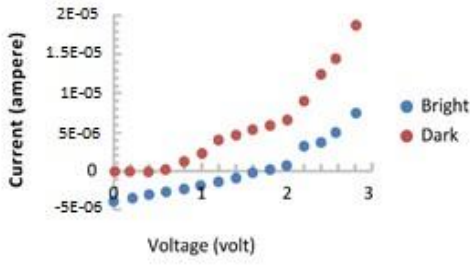
2E-05
1.5E-05
1E-05
5E-06
0
-5E-06
Current (ampere)
0 1 2 3
Voltage (volt)
Bright
Dark

(e)

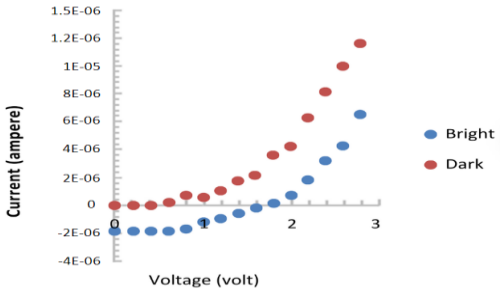
1.5E-06
1.2E-06
1E-05
8E-06
6E-06
4E-06
2E-06
0
-2E-06
-4E-06
Current (ampere)
0 1 2 3
Voltage (volt)
Bright
Dark

(f)

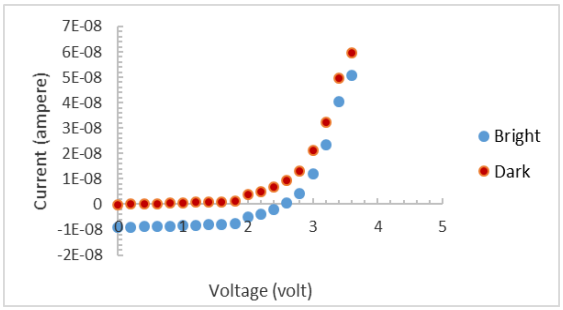
7E-08
6E-08
5E-08
4E-08
3E-08
2E-08
1E-08
0
-1E-08
-2E-08
Current (ampere)
0 1 2 3 4 5
Voltage (volt)
Bright
Dark

(g)

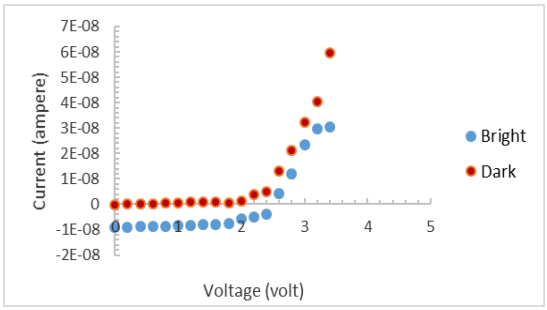
7E-08
6E-08
5E-08
4E-08
3E-08
2E-08
1E-08
0
-1E-08
-2E-08
Current (ampere)
0 1 2 3 4 5
Voltage (volt)
Bright
Dark

(h)

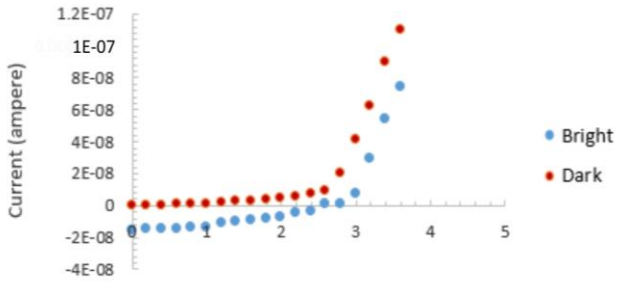
1.2E-07
1E-07
8E-08
6E-08
4E-08
2E-08
0
-2E-08
-4E-08
Current (ampere)
0 1 2 3 4 5
Bright
Dark

(i)

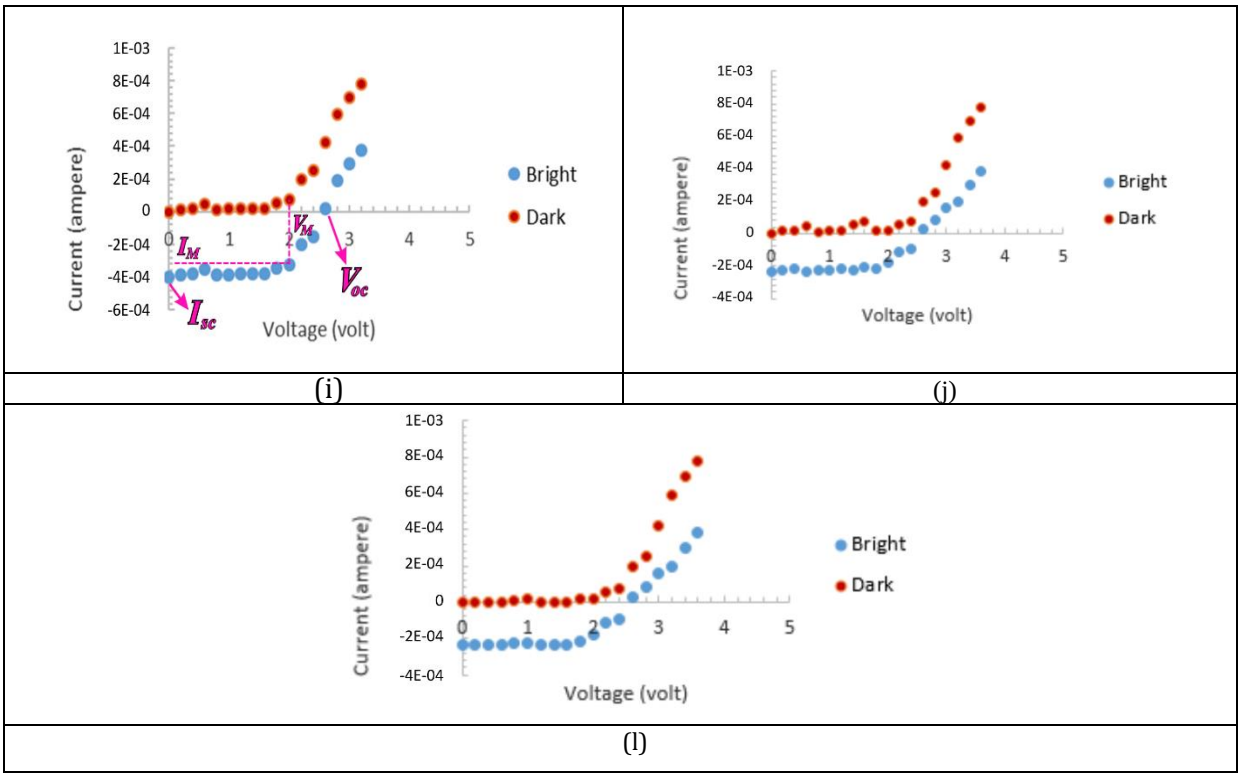

Figure. 18. The I-V curve of (a) 0% Li(CH_3COO) repetition 1; (b) 0% Li(CH_3COO) repetition 2; (c) 0% Li(CH_3COO) repetition 3; (d) 0.5% Li(CH_3COO) repetition 1; (e) 0.5% Li(CH_3COO) repetition 2; (f) 0.5% Li(CH_3COO) repetition 3; (g) 1% Li(CH_3COO) repetition 1; (h) 1% Li(CH_3COO) repetition 2; (i) 1% Li(CH_3COO) repetition 3; (j) 1.5% Li(CH_3COO) repetition 1; (k) 1.5% Li(CH_3COO) repetition 2; (l) 1.5% Li(CH_3COO) repetition 3

The I-V curve of the solar cell in Figure 18 is very important because the film can be claimed as a solar cell if the film device is measured in dark conditions. Then the behaviour of the rectifier (I-V curve like a normal diode) can be seen. If it fails to exhibit "solar cell" rectifying behaviour, even in the dark, it can be concluded that this film material behaves more like a resistor. Based on this statement, it can be seen that Figure 18 shows the behaviour of a rectifier (I-V curve like a normal diode) when it is in dark. Even Figure 18 shows a shift in the I-V curve due to the light illumination received by the film. The light causes the I-V curve of the film to fall from the first to the fourth quadrant. Among four variations of lithium extruders, films with a variation of 1.5% showed better I-V results than the other variations. Besides showing the behaviour of rectifier changes, the difference between the resulting current versus the resulting voltage is better than in other devices. The tests were carried out as shown in Figure 16(b). Based on this, it can be concluded that the $BaTiO_3$/Si(100) thin films in Lithium have a great potential as solar cells, especially films with a 1.5% barrier.

4. CONCLUSION

The energy gap value of the thin film decreases due to the increase in lithium doping. The dopant donor atom causes the allowable energy level to be slightly below the conduction band. The presence of new bands causes the energy gap to decrease. The morphological properties of the $BaTiO_3$/Si(100) thin film have fairly homogeneous grains with the addition of lithium acetate as a binder into barium titanate; The grain size decreases because the lithium-ion radius is smaller than the barium ion radius. I-V measurements and simulation of thin films as solar cells show that the values of Voc, Isc, FF and efficiency increase with doping. At the I-V curve test, light causes the I-V curve of the film to fall from the first to the fourth quadrant. Of the four variations of lithium, the film with a variation of 1.5% showed better I-V results compared to the other variations. As well as demonstrating a change in rectifier behavior, the difference between the generated current versus the output voltage is more subtle than other devices. Based on this, it can be concluded that lithium-doped $BaTiO_3$/Si(100) thin films have great potential as solar cells, especially layers with 1.5% doping. The values of Voc, Isc, FF and the efficiency obtained by a film with 1.5% doping are Voc = 2.60 volts; Isc = 0.40 mA; FF = 0.63; and η = 0.65% with a solar cell area of 1 cm^2 when exposed to light of 1000 Wm^{-2}. This strengthens the statement from the test results above that a thin layer of BaTiO3/Si(100) has promising future for solar cell research and development.

ACKNOWLEDGMENTS

The Research Grant funded this research for the Collaborative Research Program Jambi University and IPB University from Rector IPB University with contract number: 2168/UN21.11/PT.01.05/SPK/2022 on 2 June 2022.

REFERENCES

[1] Irzaman, Ridwan Siskandar, "Integrated Ferroelectrics," vol. 168, issue 1, pp. 130-150, 2016.
[2] Irzaman et al., "Biointerface Res. Appl. Chem.," vol. 11, no. 6, pp. 14956–14963, 2021.
[3] Hamdani, M. Komaro, and Irzaman, "Mater. Phys.

Mech.," vol. 42, no. 1, pp. 131–140, 2019.
[4] H. He, X. Lu, E. Hanc, C. Chen, H. Zhang, and L. Lu, "J. Mater. Chem. C," vol. 8, no. 5, pp. 1494–1516, 2020.
[5] A. Karvounis, F. Timpu, V. V. Vogler-Neuling, R. Savo, and R. Grange, "Adv. Opt. Mater.," vol. 8, no. 24, pp. 1–23, 2020.
[6] R. Siskandar, F. C. Dio, H. Alatas, and Irzaman, "BIOINTERFACE Res. Appl. Chem.," vol. 12, no. 2, pp. 2138–2151, 2022.
[7] Irzaman, Ridwan Siskandar, Brian Yuliarto, Mochammad Zakki Fahmi, Ferdiansjah, "chemosensor," vol. 3, no. 8, pp. 1–11, 2020.
[8] M. Dahrul, "Pendadahan, Karakterisasi dan Aplikasi Film Tipis Ba0,5Sr0,5TiO3 Sebagai Pengukur Konsentrasi Gula," 2011.
[9] S. W. Konsago, K. Žiberna, B. Kmet, A. Benčan, H. Uršič, and B. Malič, "Molecules," vol. 27, no. 12, pp. 3753, 2022.
[10] M. Falmbigl et al., "J. Phys. Chem. C," vol. 121, no. 31, pp. 16911–16920, 2017.
[11] Y. R. Liu et al., "Nanomaterials," vol. 12, no. 2397, pp. 1–11, 2022.
[12] S. I. Gudkov, A. V. Solnyshkin, D. A. Kiselev, and A. N. Belov, "Ceramica," vol. 66, no. 379, pp. 291–296, 2020.
[13] Y. Iriani, L. Setyaningsih, and A. Jamaluddin, "Indonesian Journal of Applied Physics," vol. 2, no. 2, pp. 170–175, 2012.
[14] A. M. Moreira Ficanha, A. Antunes, C. E. Demaman Oro, R. M. Dallago, and M. L. Mignoni, "BIOINTERFACE Research and Applied Chemistry," vol. 10, no. 6, pp. 6744–6756, 2020.
[15] B. K. Swamy et al., "BIOINTERFACE Research and Applied Chemistry," vol. 10, no. 5, pp. 6460–6473, 2020.
[16] P. L. Bintari et al., "Key Engineering Materials," vol. 855 KEM, pp. 208–212, 2020.
[17] X. Tang et al., "Journal of the European Ceramic Society," vol. 42, no. 1, pp. 175–180, 2022.
[18] Y. Iriani, F. Nurosyid, and A. U. L. S. Setyadi, "AIP Conference Proceedings," vol. 2296, 2020.
[19] U. Anindy, M. Nur Indro, and I. Husein, "Ferroelectrics," vol. 570, no. 1, pp. 162–175, 2021.
[20] Irzaman et al., "Ferroelectrics," vol. 524, no. 1, pp. 44–55, 2018.
[21] Irzaman et al., "Journal of King Saud University - Science," vol. 34, no. 6, pp. 102180, 2022.
[22] J. N. Mirdda, S. Mukhopadhyay, K. R. Sahu, and M. N. Goswami, "Biointerface Research and Applied Chemistry," vol. 12, no. 6, pp. 7927–7941, 2022.
[23] M. Arshad et al., "Ceramics International," vol. 46, no. 2, pp. 2238–2246, 2020.
[24] A. Ismangil and W. G. Prakoso, "International Journal of Advanced Science and Technology," vol. 29, no. 6, pp. 3234–3240, 2020.
[25] Nani Djohan et al., "International Journal of Nanoelectronics and Materials," vol. 15, no. 1, pp. 17–26, 2022.
[26] Hidayatul Fitriya et al., "Jurnal Pembelajaran Fisika," vol. 5, no. 4, pp. 343–350, 2017.
[27] Ervayenri et al., "Jurnal Karya Ilmiah Multidisiplin," vol. 3, no. 1, pp. 95–101, 2023.
[28] Muhammad Ilham Maulana et al., "Jurnal Teknik Mesin Unsyiah," vol. 6, no. 1, pp. 1–6, 2018.